Translational mobilities of proteins in nanochannels: A coarse-grained molecular dynamics study

Navaneeth Haridasan,[1] Sridhar Kumar Kannam,[2,3] Santosh Mogurampelly,[4] and Sarith P. Sathian[1,*]

[1]*Department of Applied Mechanics, Indian Institute of Technology Madras, Chennai 600036, India*
[2]*Faculty of Science, Engineering and Technology, Swinburne University of Technology, Hawthorn, Victoria 3122, Australia*
[3]*School of Sciences, RMIT University, Melbourne, Victoria 3001, Australia*
[4]*Institute for Computational Molecular Science, Temple University, Philadelphia, Pennsylvania 19122, USA*

We investigated the translation of a protein through model nanopores using coarse-grained (CG) nonequilibrium molecular dynamics (NEMD) simulations and compared the mobilities with those obtained from previous coarse-grained equilibrium molecular dynamics model. We considered the effects of nanopore confinement and external force on the translation of streptavidin through nanopores of dimensions representative of experiments. As the nanopore radius approaches the protein hydrodynamic radius, $r_h/r_p \to 1$ (where r_h is the hydrodynamic radius of protein and r_p is the pore radius), the translation times are observed to increase by two orders of magnitude. The translation times are found to be in good agreement with the one-dimensional biased diffusion model. The results presented in this paper provide useful insights on nanopore designs intended to control the motion of biomolecules.

I. INTRODUCTION

Macromolecular transport is ubiquitous in living organisms where biopolymers such as proteins move from one region to another in a crowded environment [1,2]. Initial experimental observations of poly(ethylene glycol) [3] and single-stranded DNA [4] translocation in naturally occurring ion channels have generated huge interests in polymer translocations [5–7]. Since then, understanding the macromolecular basis of polymer translocation has emerged as a major research activity [8–11].

Many experimental techniques have been developed in the past few decades for isolating and characterizing biopolymers at the single molecular level [12,13]. Nanopore sensors based on resistive pulse sensing techniques are cost-effective and relatively easy to use compared to the biological assays for investigating at the single molecules level in real time [7,14]. These devices measure the variation in ionic current when a biomolecule contained in an electrolyte solution translocates through a nanopore. The properties of molecules such as size, charge, conformation, concentration, etc., can be inferred by measuring the translocation time, drop in the current, and frequency of translocation events [5,6,8,15–19]. These sensors have a wide range of potential applications in drug screening and delivery, pharmacology, molecular biology, etc. [6,7,10,20].

Several experiments have investigated macromolecular translocation and sensing using synthetic nanopores [21–24]. Large translocation velocities of biomolecules poses a serious challenge to nanopore sensors [16–18,25,26]. For instance, it is infeasible to detect high-velocity translocation events due to practical limitations such as insufficient bandwidth of the sensing devices [24]. Therefore, it is imperative to either enhance the temporal resolution of detection or slow down the velocity, broadening the use of nanopore sensing technology to a wide range of applications. For the latter, a fundamental understanding of the factors governing the directional motion of biomolecules is necessary, and hence this study.

The first theoretical work on polymer translocation [27] was concurrently published with the first experimental work on macromolecular translocation [4]. This theoretical work was further developed shortly afterward [28]. Both these models considered the polymer translocation as a one-dimensional diffusion problem of a long and flexible polymer chain assuming it to be in quasiequilibrium. But in typical translocation experiments, the macromolecular movement in nanopores is always assisted by an external force, hence it will not comply with quasistatic assumption [29]. A general formalism for the forced translocation phenomena based on force balance of drag and applied force was proposed later [30].

Researchers have modeled protein translocation by a one-dimensional (1D) Langevin equation [5,19,31] and reported that the translocation phenomenon is mainly influenced by hydrodynamic drag experienced by the molecule inside the nanopore as well as its interaction with the nanopore. Therefore, regulating the nanopore interactions along with increasing solvent viscosity, reducing the temperature, etc. [32], could be a promising approach toward efficient sensing. We refer to Keyser [14] for a comprehensive review on strategies in controlling the nanopore transport.

Kannam and Downton [33] used coarse-grained equilibrium molecular dynamics (CGEMD) simulations to examine the effect of hydrodynamics on the diffusion of proteins confined in nanopores. It was demonstrated that choosing comparable sizes of pore to the protein is particularly advantageous for reducing the protein diffusion and hence to increase the sensor efficiency. In this work, we apply a range of external forces on the protein and examine the translational motion.
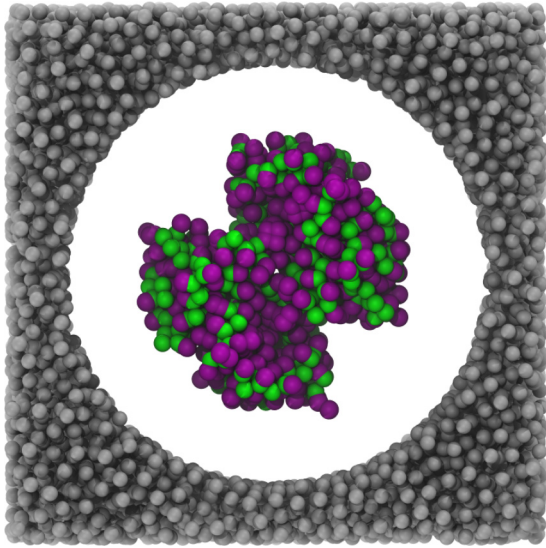
*sarith@iitm.ac.in

FIG. 1. Coarse-grained model of the protein streptavidin (PDB code: 4JO6 [36]), confined in a nanopore of radius 5 nm. The nanopore, protein backbone, and side chains are colored in gray, green, and purple, respectively. The solvent is not shown for visual clarity.

The external force can be regarded as an overall effect of electrophoretic force on the protein. The effects arising from partial atomic charges on different segments of proteins are not considered [19]. Comparison of the translational mobility influenced by external force and pore diameter with those of the CGEMD model mentioned above and translation time distribution correspondence with a continuum model forms the core of this research.

II. SIMULATION DETAILS

The interactions between coarse-grained beads are modeled using the Martini force field [34,35]. The protein streptavidin (PDB code: 4JO6 [36]) is coarse-grained at the residue level (Fig. 1) and each solvent bead represents four water molecules. The protein is solvated in a solvent box with its center of mass (c.m.) tethered to the box center. The system is equilibrated in the N-P-T ensemble at 300 K temperature and 1 bar pressure using a Berendsen thermostat and barostat, respectively. In the next step, the nanopore is created by freezing the solvent beads outside the required pore region in such a way that the pore and z axis are aligned. The pore length is kept fixed at 20 nm and the radius r_p is varied from 4 to 12.5 nm to examine the effect of confinement on the mobility. Periodic boundary conditions were applied in all three directions making the pore infinitely long for all the simulation cases. Considering the fact that the protein is moving through an infinite length pore, the term translation is used throughout this study in lieu of translocation found in nanopore literatures.

The protein has a radius of gyration, r_g, of ~ 2.2 nm and the maximum length of protein m, considering all its orientations is ~ 6.5 nm. For the comparison with nanopores, protein size is quantified throughout the study in terms of hydrodynamic radius, r_h. The hydrodynamic or Stokes radius is defined as the radius of a hard sphere which has a bulk diffusion coefficient equivalent to the protein under similar simulation

conditions. r_h is estimated as 3.22 nm from Stokes-Einstein relationship, $D_t^\infty = k_b T / 6\pi \eta r_h$, where the viscosity [33] η (1.01 cP) of the solvent and finite-size corrected bulk diffusion coefficient [37] D_t^∞ (0.0682 nm²/ns) were calculated from equilibrium molecular dynamics simulations of protein in bulk. The protein is forced through the pore by applying external forces corresponding to accelerations a_z in the range of 1.0–5.0 (10^{-3} nm/ps²). For brevity, we use the values of acceleration throughout this paper to represent the force applied on the protein. To avoid the protein adsorption to the nanopore, the protein's c.m. is tethered in the radial direction to the pore axis by using a harmonic potential with a force constant 12 kcal mol^{-1} Å^{-2}. Hence the protein is free to move in the z direction and restrained to move in the x and y directions. No restraints are applied on the rotational degree of freedom of the protein. The production simulations are carried out in the N-V-T ensemble with a time step of 20 fs for 200 ns using the GROMACS [38] simulation package. The simulation models and protocols are adapted from Kannam and Downton [33].

III. RESULTS AND DISCUSSION

A. Conformational stability of the protein

In the translocation experiments at physiological conditions, globular proteins are generally proclaimed to maintain its conformation without any significant changes [19,39]. But in NEMD simulations, the proteins are reported to undergo conformational changes due to the large external forces [40–42]. To measure the conformational stability of the protein, we measured the root-mean-square deviation (RMSD) and the radius of gyration (r_g) during the translation in our NEMD simulations.

RMSD is a measure of the protein's conformational change which is calculated as the root-mean-square deviation of the protein's atom positions with respect to a reference structure.

$$\text{RMSD}(t) = \sqrt{\frac{1}{N} \sum_{i=1}^{N} \left[\mathbf{r}_i(t) - \mathbf{r}_i^{\text{ref}} \right]^2}, \qquad (1)$$

where N is the number of atoms in the protein. The $\mathbf{r}_i(t)$ represents the position vector of the ith atom at time t and $\mathbf{r}_i^{\text{ref}}$ denotes its reference structure position vector. The radius of gyration, $r_g = \sqrt{\frac{1}{N} \sum_{i=1}^{N} (\mathbf{r}_i - \mathbf{r}_{\text{c.m.}})^2}$ of the protein, on the other hand, quantifies its globular size providing an alternate quantification of the protein's conformational changes. The time evolution of RMSD and r_g is shown in Figs. 2(a) and 2(b) as the protein translocates through the pore, at an applied force corresponding to the acceleration 1.0 (10^{-3} nm/ps²). We find no significant deviation in the conformational state of the protein, indicating that the magnitudes of external forces considered in the NEMD simulations are reasonably appropriate to investigate the translation phenomena. Similar observations were made at the other accelerations encountered in this study.
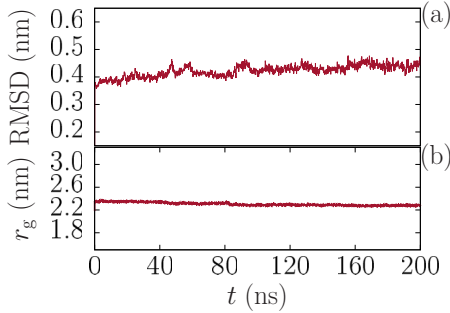
FIG. 2. (a) RMSD and the (b) radius of gyration (r_g) of streptavidin with time during the translation at an acceleration of 1.0 (10^{-3} nm/ps^2) in NEMD simulation.

B. Translation process and mobilities

Previous studies reported that proteins could be adsorbed on the nanopore surface which significantly increases the translocation time, induce conformational changes, and even trigger the activation of binding sites of the protein [43–47]. While it is important to understand such effects, we simplified our model by tethering the c.m. of the protein to the pore axis with a harmonic potential, to primarily study the translation mechanism without the protein adsorbing to the pore surface.

In Fig. 3(a), we show the instantaneous c.m. position of the protein along the pore axis, z, in ten independent simulations for a pore radius of 4.5 nm and at an external force corresponding to acceleration of 1.0 (10^{-3} nm/ps^2). For a given trajectory, we observe that z exhibits local fluctuations on short timescales corresponding to protein's typical random
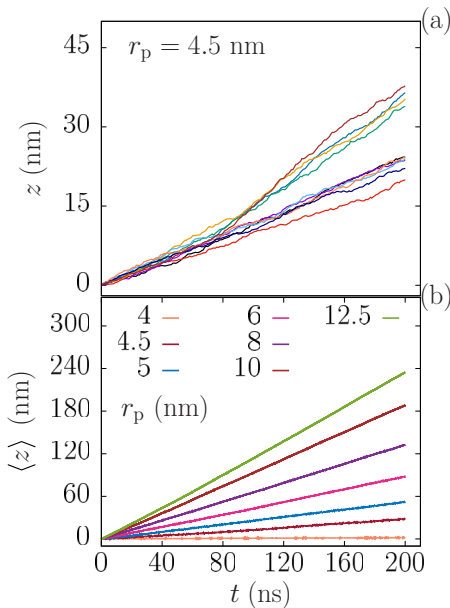

FIG. 3. (a) The instantaneous center-of-mass position of streptavidin along the pore axis, z, with time for ten replica simulations for a pore radius of 4.5 nm and at an acceleration of 1.0 (10^{-3} nm/ps^2). (b) The evolution of the average center-of-mass position of streptavidin along the pore axis, $\langle z \rangle$, at different pore radii ranging between 4 and 12.5 nm.
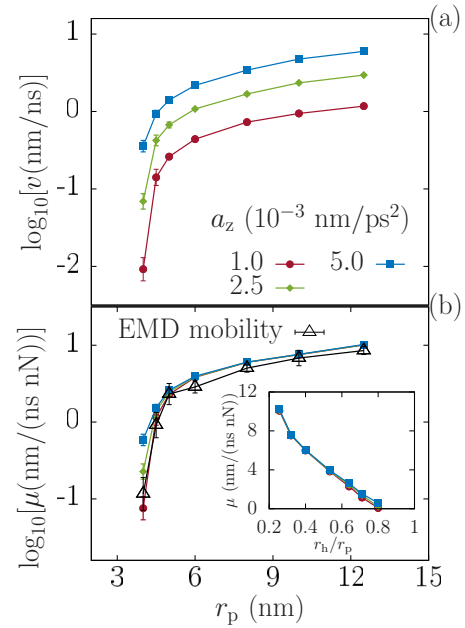

FIG. 4. (a) The average translation velocity v of protein as a function of the pore radius at different accelerations corresponding to external forces. (b) Comparison of average mobility μ calculated from nonequilibrium MD simulations [legends are the same as Fig. 4(a)] with the Einstein-Smoluchowski predictions as in Eq. (2) (triangles).

walk in a thermal environment. Due to the external force, the protein translocates along the pore axis with a net velocity. From the independent simulations for particular values of applied external force and pore radii, the velocities based on z were calculated and averaged to get a mean velocity. The error bars in Fig. 4(a) represent the standard deviation of the mean velocity values calculated from independent simulations. A t test [48] was adopted to ensure that the calculated mean value represents the population mean with sufficient confidence. For the case with largest standard deviation, it was found that the margin of error is around 10% of the mean value at a confidence level of 90%. Thus we conclude that the calculated mean value represents the population mean value with the error of 10% or less at 90% confidence.

While the observation of protein translation is quite natural because of the applied force, the effects of pore radius on protein dynamics are found to be significant, as shown in Fig. 3(b). The linearity of the average c.m. position of the protein along the pore axis, $\langle z \rangle$, indicates that the velocity is constant throughout the nanopore of any radius, r_p. The higher strength of protein-nanopore interactions with decreasing pore radius is seen to reduce the protein displacements significantly. Notably, in a nanopore of the smaller radius considered in our simulations, the protein is observed to displace barely about its size during the entire 200 ns trajectory. On the other hand, for the largest radius considered, the protein displaces approximately $100 r_g$ in 200 ns, which is two orders greater than the average displacement of protein in bulk due to diffusion (based on the Péclet number calculation defined later).

The above results demonstrate that there are considerable variations in protein displacements depending on the pore radius at a given applied force. To understand the dynamics

of the protein, the mean velocity v calculated using $\langle z \rangle$ is displayed in Fig. 4(a) at different applied forces. Consistent with the variations in $\langle z \rangle$, the velocities are seen to change significantly with the pore radius. The change of velocity is observed to span an order of magnitude below a critical pore radius, r_p^c, and approaches a constant value for $r_p > r_p^c$. This reveals the effect of pore friction on the translation velocity and consequently the translation time. This is similar to the translocation dynamics of polymer chains where the pore friction increases with a decrease of pore diameter and dominates as a finite-size effect especially for a short polymer [49]. The proportional relation between the translation velocity and external forces obtained from the simulations suggests that the forces used are in the linear regime.

Another interesting feature observed from Fig. 4(a) is that the qualitative differences in velocity with r_p are almost identical at given external forces. To quantify such a behavior, we calculated the mobility, μ, as the ratio of velocity to the applied force and the results are displayed in Fig. 4(b). Following the qualitative features observed for the velocities, we find that the mobilities are independent of the applied force for $r_p > 4$ nm, which is consistent with the experimental observation that the biopolymer electrophoretic mobilities are independent of the applied electric fields both in free solution [50] and in a translocation setup [51]. However, the mobility significantly decreases as r_p equals 4 nm or in general as it approaches the dimensions of the protein.

The translation mobilities calculated from the velocities can be directly compared [52,53] with the predictions of the Einstein-Smoluchowski relation:

$$\mu(r_p) = D(r_p)/k_B T, \tag{2}$$

where $D(r_p)$ is the diffusion coefficient of the protein in a nanopore of radius r_p, k_B is the Boltzmann constant, and T is the temperature in Kelvin. Assuming that the $D(r_p)$ is independent of the applied force [54], we evaluated $\mu(r_p)$ by using the respective $D(r_p)$ obtained under the equilibrium conditions [33]. Interestingly, we observe an excellent agreement between the μ obtained from the NEMD simulations and the EMD-based Einstein-Smoluchowski predictions.

The comparison of mobilities from EMD and NEMD simulations in Fig. 4(b) indicates that quantitatively the system exhibits similar behavior in terms of diffusion and external forcing velocity when the pore diameter is varied. From the mean values and error bars from Fig. 5, it can be observed that EMD and NEMD mobilities lie very close to each other for r_p values other than 4 nm ($r_h/r_p = 0.805$). This equivalence is applicable even for large forces considered in the simulation where diffusion timescales are almost two orders lesser than forced translation timescales. (The two-order difference between transport rates is quantified by Péclet number Pe for the protein, defined as the ratio of forced translation rate to diffusion transport rate, Pe $= \frac{r_h v(r_p)}{D(r_p)}$ where $v(r_p)$ is the velocity due to external force). Apparently, it can be safely assumed that the equivalence between EMD and NEMD mobilities prevails for any external forces between equilibrium and the forces considered in the simulation. This is not the case with pore sizes close to r_h considered in the simulation as shown in Figs. 4(b) and 5. There is a marked variation of mobility experienced
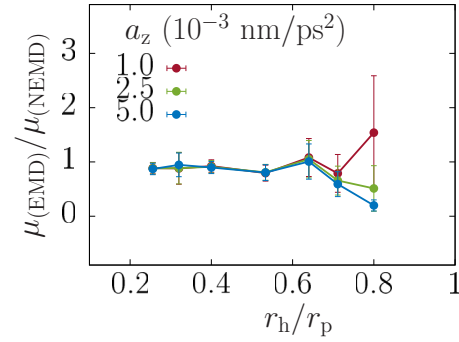

FIG. 5. Ratio of EMD to NEMD mobilities for different pore sizes and applied forces. There is a marked variation of the ratio with respect to the applied forces when the pore size is closer to protein dimensions.

by the protein with respect to the applied force for r_p value 4 ($r_h/r_p = 0.805$). This indicates that the mobility values depend on the force applied, which signifies the presence of excessive drag compared to other pores in the study. A similar observation has been made before in the literature for DNA translocation [55].

C. Probability distribution function of translation times

Numerous attempts were made previously to theoretically formulate the distribution of translocation times [41,56–58]. Among these, Talaga *et al.* [41] proposed a biased 1D Fokker-Planck diffusion model with relatively realistic boundary conditions which was later corrected as Schrödinger's first passage probability distribution function (FP-PDF) [58,59].

Following the arguments and the treatment of Talaga and Li [41,58,59], we use 1D FP-PDF to broadly describe the translation of protein through nanopores under the influence of a constant force. Since the mobilities from EMD and NEMD are equivalent from Fig. 4(b), we use Eq. (2) and velocity-force relation of mobility from NEMD to replace diffusion coefficient D of the original 1D FP-PDF. For the translation, the protein has to travel a distance l in time t, with an induced velocity v. Due to the stochastic nature of the translation process, the time required to translocate distance l assumes a probability distribution, $p(t)$, given by

$$p(t) = \left[\frac{l^2 F}{4\pi k_B T v t^3} \right]^{1/2} e^{-F(l-tv)^2/4k_B T v t}. \tag{3}$$

In the above equation, we chose $l = 50$ nm and F as the external force corresponding to the acceleration of 1.0 (10^{-3} nm/ps^2). The velocity is obtained by scaling the EMD mobility in Eq. (2) with F.

Figure 6 depicts $p(t)$ obtained numerically for streptavidin at different values of r_p. We observe that while the shape of $p(t)$ remains unaffected, the width and peak height changes significantly with r_p. The range of translation times calculated directly from NEMD velocities (circles) lies within the width estimated using Eq. (3). Moreover, the NEMD values are centered around the higher probability region for most cases of r_p. However, as the protein is restrained to the nanopore axis, the translation process is smooth without the adsorption on pore walls. Also the capture phenomena of the protein
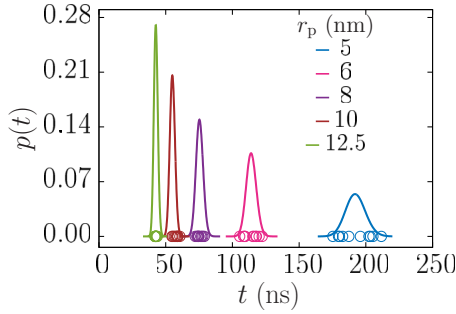
FIG. 6. Probability distribution $p(t)$ of translation times at different r_p obtained numerically using Eq. (3) for streptavidin in nanopores for F correseponding to external acceleration of 1.0 (10^{-3} nm/ps^2). The circles indicate the translation times calculated with the velocities obtained from ten independent NEMD trajectories, and agrees well with the EMD-based predictions using Eq. (3). Note that due to the limitations on computational requirements (a typical problem associated with simulations), we were not able to compute $p(t)$ directly from NEMD simulations which require roughly 10^3–10^4 independent trajectories.

is not modeled within our framework, hence unsuccessful translocation events or collisions [60] are not accounted for during the entire simulation. This may lead to an under-representation of the long tail of translation times observed in experiments [4,24,39].

Another interesting property relevant for the translation experiments is the mean translation time, τ, which can be calculated numerically by using the probability distributions as

$$\tau = \frac{\int_0^\infty t p(t) dt}{\int_0^\infty p(t) dt}. \qquad (4)$$

A comparison of τ calculated using Eq. (4) and those obtained directly from NEMD simulations is presented in Fig. 7 at different values of r_p and external forces. In the figure, $\tau_{(r_p=\infty)}$ denotes the time required for the protein to travel l for $r_p = \infty$, which is extracted by fitting the data to $\tau_0 e^{\lambda(r_h/r_p)} + \tau_{(r_p=\infty)}$, where τ_0 and λ are fitting parameters. The mean translation times calculated from NEMD simulations are seen to decrease rapidly with nanopore radius and approaches $\tau_{(r_p=\infty)}$ as shown
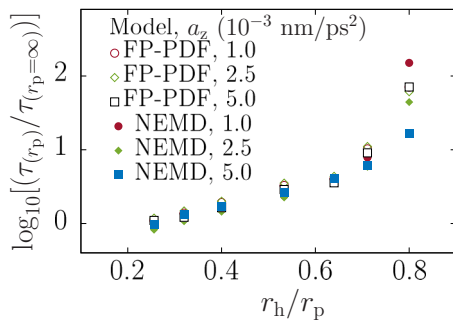

FIG. 7. Translation time τ dependency on nanopore radius. Data for NEMD simulations and 1D diffusion model at different applied forces collapses on a universal curve. Translation times evaluated using Eq. (4) (1D model) agrees with those obtained from the NEMD simulations.
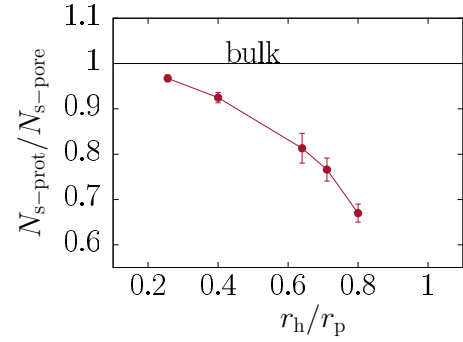

FIG. 8. Ratio of the number of solvent beads per nanometer for the distance occupied by the protein in the z direction $N_{s\text{-prot}}$, to the number of solvent beads per nanometer for the rest of the pore length $N_{s\text{-pore}}$ versus pore radii. The ratio indirectly indicates the volume occupied by the protein in comparison to solvent, if the pore length is exactly the z dimension of the protein.

in Fig. 7. The translation times predicted from the 1D FP-PDF model agree well with the NEMD results for most values of r_p, although it differs for pores similar in size to the protein. Moreover, the changes in τ with r_p are consistent with the results presented in Fig. 4(a). Additionally, the qualitative features of τ are very similar to those reported for voltage-driven DNA translocation through solid-state nanopores [60].

The ability of the 1D diffusion model in predicting the qualitative features of τ and capturing the physics of translation are promising despite ignoring details such as electro-osmotic gradients, electrostatic charge distribution, the shape of protein, etc. Overall, the qualitative agreement between the 1D diffusion model and NEMD simulations helps in rationalizing the significance of diffusion-dependent mechanisms in governing the translation of proteins in nanopores.

D. Nature of drag on the protein

An interesting question will be the source of increase in drag on the protein as the pore diameter approaches hydrodynamic radius, r_h. From Figs. 7 and 5, it is evident that for the pores with least two diameters considered in the simulation, there is a disparity with respect to velocity or time required for the protein translation. This is in line with the diffusion coefficient variation related to change in pore size expressed in a previous EMD study [33]. While most of the protein translation times corresponding to different pore sizes follow the frictional drag relationship [$\sim r_h/(r_p - r_h)$] [60], cases of r_p with 4 and 4.5 (r_h/r_p value 0.805 and 0.716, respectively) show considerable deviation from this relation. Thus, it can be inferred that, for large pores the drag is mainly a hydrodynamic effect but as r_h approaches r_p, there may be additional effects which contribute to the drag on the protein.

The ratio of the number of solvent beads per nm for the distance occupied by the protein in the z direction $N_{s\text{-prot}}$ to the number of solvent beads per nanometer for the rest of the pore length $N_{s\text{-pore}}$ is plotted against different pore radii in Fig. 8. This indicates the number of solvent beads occupying the pore volume along with the protein, if the pore length is exactly the z dimension of the protein. From Fig. 8, it is observed that for a given z dimension of the protein, the number of solvent beads
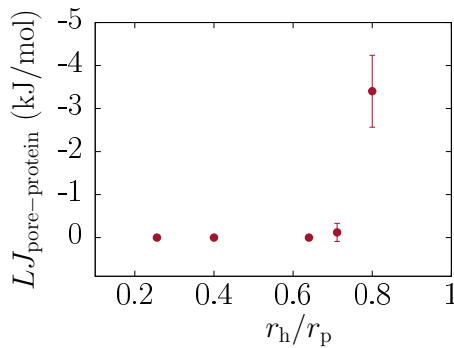
FIG. 9. Nonbonded interaction between the pore and protein for different pore sizes. r_p 4 and 4.5 nm (r_h/r_p value 0.805 and 0.716, respectively) exhibits non-negligible values of interaction compared to other values of r_p considered.

is just two times the number of protein beads for the least pore diameter. This leads to the inference that the protein occupies considerable volume inside the pore in comparison to solvent beads. Most importantly, since the maximum dimension m of the protein is around 6.5 nm throughout the simulation, for the least pore diameter case, the solvent may form a thin film between the pore and the protein or sparsely distributed solvent clusters may exist between the protein and the nanopore surface.

Apart from the above analysis, accounting for the non-bonded interaction between the pore and protein as shown in Fig. 9 reveals that there is a non-negligible interaction between the pore and protein for the case of two nanopores with the least diameters considered in the study. Thus the drag may be caused due to the presence of a thin film of solvent or due to a direct nonbonded interaction between the pore and protein, or both. While it can be speculated from the above analyses that the drag increase is mainly due to the nonbonded interaction between the protein and pore, further analyses are required for a conclusive understanding of the underlying mechanisms.

IV. CONCLUDING REMARKS AND OUTLOOK

To conclude, the mechanisms governing protein translation through nanopores are investigated in this work by considering a coarse-grained protein (streptavidin) with model nanopores using molecular dynamics simulations. To accelerate the translation process within computationally tractable timescales, we applied external forces of different magnitudes on proteins. Nanopores of varying radii ranging from 4 to 12.5 nm (r_h/r_p value 0.805 to 0.258, respectively) that are comparable to the experimental length scales are considered to understand the

effects of pore size. We simulated the translation process for ten different initial configurations to generate trajectories of 200 ns in each case.

One of the important outcomes of this paper is that the mobilities calculated from the NEMD simulations are comparable to those computed from EMD simulations indicating the similarity in system response to a wide range of forces starting from values close to equilibrium. Also, the diffusion coefficient or the mobilities depends strongly on the pore size which can be used to control the directional or diffusional motion of the protein in nanopores. As a consequence, the mean translation times are observed to be increasing rapidly with decreasing pore sizes which is in good agreement with previous experimental and simulation results [60–62].

A stochastic model based on a 1D biased diffusion equation was used to study the translation of proteins in conjunction with molecular dynamics (MD) simulations. The results of such a simplistic model are seen to corroborate the large-scale coarse-grained simulations and provide further significant insights. Specifically, the probability distributions of the translation time indicated larger standard deviations in translation time for smaller pores which are consistent with typical experimental reports [60]. More interestingly, the average translation times predicted using the stochastic model decrease rapidly with the pore size, which is in excellent agreement with NEMD simulations. Also a two-order increase of translational time signifies the presence of additional effects contributing to drag experienced by the protein, the nature of which needs to be revealed through a separate detailed study. The results presented in this paper provide useful insights on the nanopore design for several applications. For instance, the nanopore may be specifically designed to control protein diffusivity for accurate sequencing or similar applications.

Recent atomistic simulations have reported that the changes in water density fluctuations in a proton channel can potentially initiate active binding sites for the target molecules subjected to translation [43,44]. In the drug design community, such an observation is expected to generate significant interest in the quest for potential inhibitors of the proton channel. Similar phenomena could arise when protein is subjected to translation in thin nanopores, where the degree of hydration of protein becomes crucial. Explicitly, the preferential interactions between nanopores and protein's residues play a major role in the translation process. We note that while the protein is restrained along the nanopore axis in the present model, it is highly desirous to understand the importance of the solvent mediated dry-wet mechanism of protein translation process and the manner in which they are influenced by the nanopore size.

[1] M. Muthukumar, Polymer Translocation, *Investigations on the Theory of Brownian Movement* (CRC Press, Boca Raton, FL, 2011).

[2] H. Kumar, Y. Lansac, M. A. Glaser, and P. K. Maiti, Soft Matter **7**, 5898 (2011).

[3] S. M. Bezrukov, I. Vodyanoy, and V. A. Parsegian, Nature (London) **370**, 279 (1994).

[4] J. Kasianowicz, E. Brandin, D. Branton, and D. Deamer, Proc. Natl. Acad. Sci. USA **93**, 13770 (1996).

[5] C. Y. Kong and M. Muthukumar, J. Am. Chem. Soc. **127**, 18252 (2005).

[6] M. Wanunu, Phys. Life Rev. **9**, 125 (2012).

[7] F. Haque, J. Li, H.-C. Wu, X.-J. Liang, and P. Guo, Nano Today **8**, 56 (2013).

[8] H.-C. Yeh, S.-Y. Chao, Y.-P. Ho, and T.-H. Wang, Curr. Pharm. Biotech. **6**, 453 (2005).

[9] W. E. Moerner and L. Kador, Phys. Rev. Lett. **62**, 2535 (1989).

[10] S. K. Kannam, M. T. Downton, N. Gunn, S. C. Kim, P. R. Rogers, C. Schieber, J. S. Baldauf, J. M. Wagner, D. Scott, R. Bathgate, S. Skafidas, and S. Harrer, in *Micro Nano Materials, Devices, and Systems*, edited by J. Friend and H. H. Tan, Proceedings of SPIE Vol. 8923 (SPIE, Bellingham, WA, 2013), p. 89230I.

[11] B. Nandy, M. Santosh, and P. K. Maiti, J. Biosci. **37**, 457 (2012).

[12] D. R. Walt, Anal. Chem. **85**, 1258 (2013).

[13] A. A. Deniz, S. Mukhopadhyay, and E. A. Lemke, J. R. Soc., Interf. **5**, 15 (2008).

[14] U. F. Keyser, J. R. Soc., Interf. **8**, 1369 (2011).

[15] S. C. Kim, S. K. Kannam, S. Harrer, M. T. Downton, S. Moore, and J. M. Wagner, Phys. Rev. E **89**, 042702 (2014).

[16] S. Carson and M. Wanunu, Nanotechnology **26**, 074004 (2015).

[17] B. M. Venkatesan and R. Bashir, Nat. Nanotechnol. **6**, 615 (2011).

[18] A. Oukhaled, L. Bacri, M. Pastoriza-Gallego, J.-M. Betton, and J. Pelta, ACS Chem. Biol. **7**, 1935 (2012).

[19] B. Ledden, D. Fologea, D. S. Talaga, and J. Li, Sensing Single Protein Molecules with Solid-State Nanopores, in *Nanopores: Sensing and Fundamental Biological Interactions* (Springer US, New York, 2011), pp. 129–150.

[20] S. Harrer, S. C. Kim, C. Schieber, S. K. Kannam, N. Gunn, S. Moore, S. Scott, R. Bathgate, S. Skafidas, and J. M. Wagner, Nanotechnology **26**, 182502 (2015).

[21] M. M. Mohammad and L. Movileanu, Protein Sensing with Engineered Protein Nanopores, in *Nanopore-Based Technology* (Humana, New York, 2012) pp. 21–37.

[22] J. Larkin, R. Y. Henley, M. Muthukumar, J. K. Rosenstein, and M. Wanunu, Biophys. J. **106**, 696 (2014).

[23] E. L. Bonome, R. Lepore, D. Raimondo, F. Cecconi, A. Tramontano, and M. Chinappi, J. Phys. Chem. B **119**, 5815 (2015).

[24] C. Plesa, S. W. Kowalczyk, R. Zinsmeester, A. Y. Grosberg, Y. Rabin, and C. Dekker, Nano Lett. **13**, 658 (2013).

[25] Y. Feng, Y. Zhang, C. Ying, D. Wang, and C. Du, Genom. Proteom. Bioinf. **13**, 4 (2015).

[26] R. D. Maitra, J. Kim, and W. B. Dunbar, Electrophoresis **33**, 3418 (2012).

[27] W. Sung and P. J. Park, Phys. Rev. Lett. **77**, 783 (1996).

[28] M. Muthukumar, J. Chem. Phys. **111**, 10371 (1999).

[29] Y. Kantor and M. Kardar, Phys. Rev. E **69**, 021806 (2004).

[30] A. J. Storm, C. Storm, J. Chen, H. Zandbergen, J.-F. Joanny, and C. Dekker, Nano Lett. **5**, 1193 (2005).

[31] M. Muthukumar, J. Chem. Phys. **141**, 081104 (2014).

[32] D. Fologea, J. Uplinger, B. Thomas, D. S. McNabb, and J. Li, Nano Lett. **5**, 1734 (2005).

[33] S. K. Kannam and M. T. Downton, J. Chem. Phys. **146**, 054108 (2017).

[34] S. J. Marrink, A. H. de Vries, and A. E. Mark, J. Phys. Chem. B **108**, 750 (2004).

[35] S. J. Marrink, H. J. Risselada, S. Yefimov, D. P. Tieleman, and A. H. de Vries, J. Phys. Chem. B **111**, 7812 (2007).

[36] I. H. Barrette-Ng, S.-C. Wu, W.-M. Tjia, S.-L. Wong, and K. K. S. Ng, Acta Cryst. D **69**, 879 (2013).

[37] B. Dünweg and K. Kremer, J. Chem. Phys. **99**, 6983 (1993).

[38] H. J. Berendsen, D. van der Spoel, and R. van Drunen, Comput. Phys. Commun. **91**, 43 (1995).

[39] D. Fologea, B. Ledden, D. S. McNabb, and J. Li, Appl. Phys. Lett. **91**, 053901 (2007).

[40] S. K. Kannam, S. C. Kim, P. R. Rogers, N. Gunn, J. Wagner, S. Harrer, and M. T. Downtown, Nanotechnology **25**, 155502 (2014).

[41] D. S. Talaga and J. Li, J. Am. Chem. Soc. **131**, 9287 (2009).

[42] A. Aksimentiev, Nanoscale **2**, 468 (2010).

[43] E. Gianti, L. Delemotte, M. L. Klein, and V. Carnevale, Proc. Natl. Acad. Sci. USA **113**, E8359 (2016).

[44] S. C. van Keulen, E. Gianti, V. Carnevale, M. L. Klein, U. Rothlisberger, and L. Delemotte, J. Phys. Chem. B **121**, 3340 (2017).

[45] I. Rodriguez and S. F. Y. Li, Anal. Chim. Acta **383**, 1 (1999).

[46] N. F. Y. Durand and R. Philippe, Lab on a Chip **9**, 319 (2009).

[47] R. Carr, J. Comer, M. D. Ginsberg, and A. Aksimentiev, IEEE Trans. Nanotechnol. **10**, 75 (2011).

[48] Student, Biometrika **6**, 1 (1908).

[49] T. Ikonen, A. Bhattacharya, T. Ala-Nissila, and W. Sung, Europhys. Lett. **103**, 38001 (2013).

[50] N. C. Stellwagen, A. Bossi, C. Gelfi, and P. G. Righetti, Electrophoresis **22**, 4311 (2001).

[51] P. Chen, J. Gu, E. Brandin, Y.-R. Kim, Q. Wang, and D. Branton, Nano Lett. **4**, 2293 (2004).

[52] W. Brown and R. Rymden, Macromolecules **21**, 840 (1988).

[53] V. Pryamitsyn and V. Ganesan, J. Polym. Sci.: Polym. Phys. Ed. **54**, 2145 (2016).

[54] A. E. Nkodo, J. M. Garnier, B. Tinland, H. Ren, C. Desruisseaux, L. C. McCormick, G. Drouin, and G. W. Slater, Electrophoresis **22**, 2424 (2001).

[55] S. Carson, J. Wilson, A. Aksimentiev, and M. Wanunu, Biophys. J. **107**, 2381 (2014).

[56] D. K. Lubensky and D. R. Nelson, Biophys. J. **77**, 1824 (1999).

[57] A. Berezhkovskii and I. Gopich, Biophys. J. **84**, 787 (2003).

[58] D. Y. Ling and X. S. Ling, J. Phys.: Condens. Matter **25**, 375102 (2013).

[59] D. S. Talaga and J. Li, J. Chem. Soc. **135**, 13220 (2013).

[60] M. Wanunu, J. Sutin, B. McNally, A. Chow, and A. Meller, Biophys. J. **95**, 4716 (2008).

[61] T. Menais, S. Mossa, and A. Buhot, Sci. Rep. **6**, 38558 (2016).

[62] T. Menais, Phys. Rev. E **97**, 022501 (2018).